Journal of Power Sources 240 (2013) 544–550

Contents lists available at SciVerse ScienceDirect

Journal of Power Sources

journal homepage: www.elsevier.com/locate/jpowsour

Controlled synthesis of hierarchical polyaniline nanowires/ordered bimodal mesoporous carbon nanocomposites with high surface area for supercapacitor electrodes

Yanfang Yan [a], Qilin Cheng [a,b,*], Zhengju Zhu [a], Vladimir Pavlinek [b], Petr Saha [b], Chunzhong Li [a,*]

[a] Key Laboratory for Ultrafine Materials of Ministry of Education, School of Materials Science and Engineering, East China University of Science and Technology, 200237 Shanghai, China
[b] Centre of Polymer Systems, Polymer Centre, Tomas Bata University in Zlin, nam. T.G. Masaryka 5555, 760 01 Zlin, Czech Republic

HIGHLIGHTS

- PANI nanowires/ordered bimodal mesoporous carbon composite was synthesized.
- The hierarchical composite exhibits high surface area and bimodal pore distribution.
- The composite with 60 wt% PANI possesses a high specific capacitance of 517 F g^{-1}.

ARTICLE INFO

Article history:
Received 19 November 2012
Received in revised form
21 March 2013
Accepted 29 March 2013
Available online 10 April 2013

Keywords:
Polyaniline nanowires
Ordered bimodal mesoporous carbon
Nanocomposite
Electrochemical properties

ABSTRACT

A facile strategy is developed for the synthesis of hierarchical polyaniline nanowires/ordered bimodal mesoporous carbon (PANI/OBMC) composites via chemical oxidative polymerization. Structural and morphological characterizations indicate that the polyaniline nanowire arrays with 20–30 nm diameters are grown on the surface of the OBMC. The bimodal pore distribution and hierarchical nanostructure endow the PANI/OBMC composite with high surface area of 599 m^2 g^{-1}. Electrochemical performance of the hierarchical PANI/OBMC composite as supercapacitor electrode materials has been evaluated by cyclic voltammetry and galvanostatic charge–discharge techniques. The hierarchical composite with 60 wt% PANI possesses the highest specific capacitance of 517 F g^{-1} and outstanding cycling stability with a capacitance retention of 91.5% after 1000 cycles. The coexistence of primary mesopores and abundant small mesopores is in favor of the fast penetration of electrolyte and the unique hierarchical structure facilitates the ion diffusion and shortens the charge transfer distance, which lead to superior electrochemical performance of PANI/OBMC-60%.

1. Introduction

Supercapacitors, combining the advantages of high specific energy of rechargeable batteries and high power of dielectric capacitors, have attracted great attention in the past decades due to their wide applications in hybrid electric vehicles, backup power supplies and portable electronic devices [1–4]. Porous carbon materials, transition-metal oxides and conducting polymers are the fundamental candidates as the electrode materials for supercapacitors [1].

Among the conducting polymers, PANI is considered to be a prospective electrode material because of its low cost, ease of synthesis, and relatively high conductivity [5–7]. In particular, aligned one-dimensional nanorod or nanowire arrays of PANI have been regarded as ideal candidates owing to their large specific area and optimized ion diffusion path [8]. Vertically oriented PANI nanorods have been reported to exhibit superior electrochemical properties with a large capacitance value of 3407 F g^{-1} [9]. However, the poor cycling stability is still a major obstacle for PANI to be used in supercapacitors due to the repeated swelling and shrinking of PANI during the doping and de-doping process. Therefore, numerous research groups have consciously made efforts to synthesize composites combing the high capacitance of PANI nanostructure arrays with the excellent stability of various carbon supports for supercapacitors [10,11]. For instance, Wang et al. [12]

* Corresponding authors. Key Laboratory for Ultrafine Materials of Ministry of Education, School of Materials Science and Engineering, East China University of Science and Technology, 200237 Shanghai, China. Tel.: +86 21 64250949; fax: +86 21 64250624.
E-mail addresses: chengql@ecust.edu.cn (Q. Cheng), czli@ecust.edu.cn (C. Li).

0378-7753/$ – see front matter © 2013 Elsevier B.V. All rights reserved.
http://dx.doi.org/10.1016/j.jpowsour.2013.03.190

reported that the ordered whisker-like PANI grown on the surface of mesoporous carbon possessed high specific capacitance, but the specific surface area of the resultant composite was only 35 $m^2\ g^{-1}$ as the mesopores were filled with PANI and thus the electric double-layer capacitance of the mesoporous carbon could not be utilized sufficiently. Therefore, there is a great desire to develop a new strategy to incorporate conducting polymers into carbon materials without a significant reduction in their surface area. Then the obtained hybrid composites with high surface area can fully take advantage of the synergistic effect between two components to enhance the electrochemical performance.

Recently, ordered mesoporous carbon materials (OMC) with interconnected channel or bimodal pore distribution have been regarded as good candidates of electrode materials for supercapacitors due to their high surface area, uniform pore connections and high electrical conductivity [13,14]. The OMC with interpenetrating networks was prepared by a triconstituent co-assembly method and a great many small pores are generated in the carbon walls after the removal of silica [15]. Xia et al. found that the tri-OMC possessed much higher specific capacitance than di-OMC owing to the large ordered pore channels which are continuous connected in tri-OMC [16]. Similarly, Fu et al. reported a novel OMC with an interconnected channel structure showing better electric double layer performance as compared to the conventional OMC [17]. Furthermore, the composite of PANI and OMC with continuous interpenetrating framework exhibited an enhanced specific capacitance of 400 F g^{-1} [18]. Hence, the OMC with bimodal pore distribution would be an ideal host to prepare hybrid nanocomposites with enhanced electrochemical properties. However, there has no report dealing with hierarchical PANI nanowire/OMC with bimodal pore distribution so far.

Herein, we develop a simple strategy for the synthesis of hierarchical PANI/OBMC composites via chemical oxidative polymerization using OMC–SiO_2 as the host. The PANI nanowire arrays can be easily obtained without templates. The small mesopores inside the mesoporous carbon walls can be well reserved after removal of the SiO_2 and proper PANI content introduced can effectively retain the primary mesopores open. Therefore, the resulted hierarchical composite can exhibit bimodal pore distribution and thus possess high surface area. The morphology, pore structure and electrochemical properties were investigated in detail.

2. Experimental

2.1. Materials

Aniline (An, analytical grade) purchased from Shanghai Chemical Reagent Co. was distilled under vacuum prior to use. Triblock copolymer Pluronic F127 (M_w = 12,600, $EO_{106}PO_{70}EO_{106}$) and polytetrafluoroethylene (PTFE, 60 wt% dispersion in water) were supplied by Sigma Aldrich. Carbon black was obtained from TIMCAL Co., Swiss. Ammonium persulfate (APS, $(NH_4)_2S_2O_8$, 98%), tetraethyl orthosilicate (TEOS, ≥28%), hydrofluoric acid (HF, 40%) and other reagents were of analytical grade and used as received without further purification. The resol precursors (M_w < 500) were synthesized according to the previous method [19].

2.2. Synthesis of the hierarchical nanocomposites

Ordered mesoporous carbon–silica (OMC–SiO_2) nanocomposites were synthesized similar to the procedure reported by Zhao [15]. PANI/OBMC composites were prepared by chemical oxidation polymerization of aniline monomer in the presence of OMC–SiO_2 (synthetic route (a) shown in Fig. 1). In a typical procedure, 0.15 g OMC–SiO_2 was added into 10 ml 20 wt% ethanol solution containing 1 g H_2SO_4. The mixture was stirred for 10 min and then ultrasonicated until the OMC–SiO_2 was fully dispersed. Afterward, the aniline monomer was added to the suspension at 0 °C and stirred under vacuum for 1 h. While intensive stirring, 10 ml 20 wt% ethanol solution was added to the above solution quickly. Then the pre-cooled solution of Ammonium persulfate (APS) (the molar ratio of aniline/APS is 1:1) was added dropwise to the mixture, and the polymerization was carried out at 0 °C for 5 h. The obtained composite was washed with 10 wt% HF solution to remove SiO_2. Finally, the PANI/OBMC product was filtered, washed and dried under vacuum at 70 °C for 24 h. By changing the concentration of aniline monomer (55, 65, 75, 80, 90, 100, 150 mM) in the preparation system, composites with different PANI contents

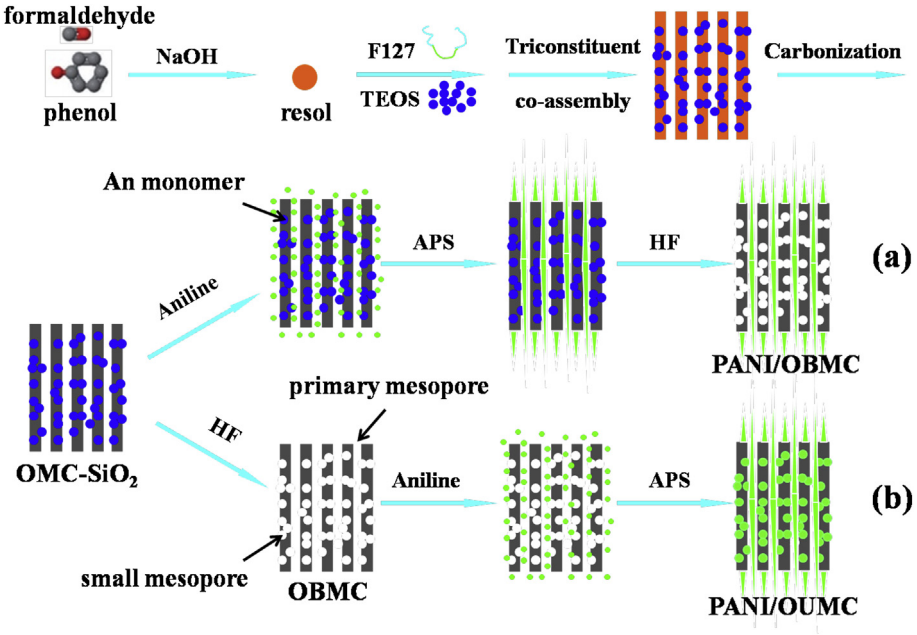

Fig. 1. Schematic illustration of the preparation process of (a) PANI/OBMC and (b) PANI/OUMC composites.

(51, 54, 60, 64, 71, 81, 86%) yielded, respectively, which were denoted as PANI/OBMC-*x*, where *x* represents the percentage of PANI in the composites. The content of PANI in the nanocomposite was evaluated by calculating the weight increase of OBMC. In comparison, polyaniline/ordered unimodal mesoporous carbon (PANI/OUMC) composite was also prepared using the similar procedure except that OBMC (i.e. SiO_2 particles were removed by HF before polymerization of aniline) was used as the host (synthetic route (b) shown in Fig. 1).

2.3. Characterization of composites

The morphology of the final composites was characterized using a field-emission scanning electron microscope (FE-SEM, HITACHI S4800) and transition electron microscopy (TEM, JEOL 2100F). X-ray diffraction (XRD) patterns were recorded on a Rigaku D/Max 2550 VB/PC X-ray diffractometer operating at 40 kV and 20 mA using Cu Kα radiation ($\lambda = 0.15406$ nm). Fourier transformation infrared spectra (FTIR) of the samples were measured from KBr sample pellets on a Nicolet 5700 spectrometer. Nitrogen adsorption–desorption isotherms were performed with an ASAP 2020 Micromeritics analyzer at 77 K and the specific surface areas (S_{BET}) were deduced by using the BET equation.

2.4. Preparation of electrodes and electrochemical measurement

The working electrodes were prepared by mixing 80 wt% active material, 10 wt% carbon black, and 10 wt% polytetrafluoroethylene (PTFE), then pressed into thin disks with uniform thickness. The mass loading of the active materials on each electrode is about 8 mg cm^{-2}. The supercapacitor was constructed by two symmetric working electrodes, sandwiched with a polypropylene (PP) separator and 1 mol L^{-1} aqueous H_2SO_4 as an electrolyte. All the electrochemical experiments in this work were carried out using a teflon swagelok type two-electrode configuration with two stainless-steel sheets as the current collector. Cyclic voltammetry (CV) experiments were conducted with a PARSTAT 2273/CS130 electrochemical station and galvanostatic charge–discharge (CD) curves and cycle stability were performed with LAND CT2001A at room temperature. The potential range for CV and CD examinations varied from 0 to 0.8 V.

3. Results and discussion

3.1. Morphology and structural characterization

The morphologies of the OBMC and the PANI/OBMC-60% composite were examined by FE-SEM. The prepared OBMC exhibits stone-like morphology with irregular shapes (Fig. 2a and b). Owing to the deposited PANI on the OBMC, the PANI/OBMC-60% composite shows a completely different morphology from OBMC in Fig. 2c. The magnified SEM image (Fig. 2d) clearly reveals that ordered PANI nanowire arrays with long length were evenly covered on the surface of OBMC. The TEM images of the OBMC shown in Fig. 3a and b feature large domains of highly ordered stripe-like and hexagonally arranged carbon nanowires viewed from the [110] and [001] directions. The results indicate well-ordered 2-D hexagonal *p6m* mesostructure can be well retained after removing the SiO_2 nanoparticles. As shown in Fig. 3c, TEM image of PANI/OBMC-60% composite illustrates plenty of PANI nanowires extended from the exterior of the OBMC into the interparticle open space. The magnification TEM image illustrates that the PANI nanowires are about 20–30 nm in diameter and 100–150 nm in length (Fig. 3d). And the inset HRTEM image of Fig. 3c demonstrates that the ordered mesoporous structures are still preserved well for the PANI/OBMC-60% composite.

The chemical structure of OMC–SiO_2, OBMC, PANI/OBMC-60% and PANI/OUMC-60% was confirmed by FTIR spectra in the 400–4000 cm^{-1} region (Fig. 4). Two broad bands at 1090 cm^{-1} and 3450 cm^{-1} are both observed in the curves of OMC–SiO_2 and OBMC, which can be attributed to the stretching vibration of the –OH and C–O bonds, respectively. In comparison to OBMC, OMC–SiO_2 shows two additional Si–O–Si stretching vibration of SiO_2 centered at 460 cm^{-1} and 791 cm^{-1}. The disappearance of

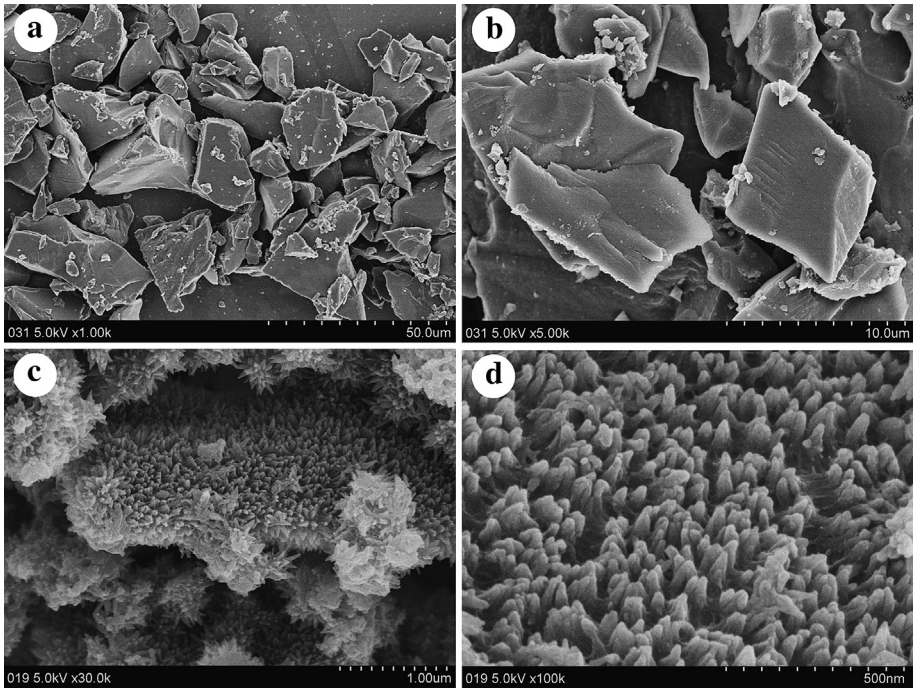

Fig. 2. (a) SEM image of OBMC. (b) High-magnification SEM image of OBMC. (c) SEM image of PANI/OBMC-60%. (d) High-magnification SEM image of PANI/OBMC-60%.

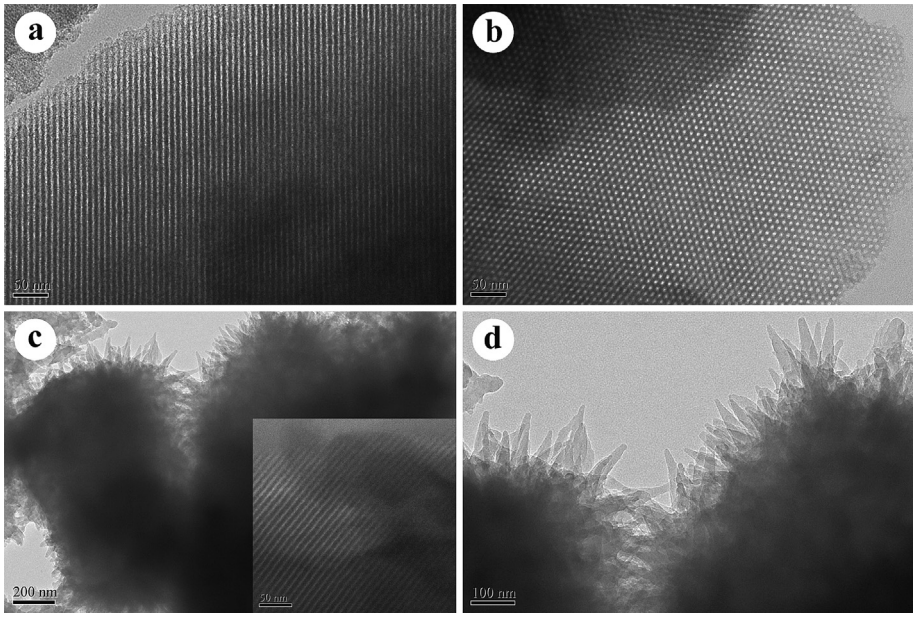

Fig. 3. (a) HRTEM image of OBMC viewed from the [110] direction. (b) HRTEM image of OBMC viewed from the [001] direction. (c) TEM image of PANI/OBMC-60% (inset is the HRTEM image of PANI/OBMC-60%). (d) High-magnification TEM image of PANI/OBMC-60%.

characteristic peaks of SiO_2 in OBMC demonstrates that SiO_2 nanoparticles have been completely removed by HF. As shown in the curves of the composites, the characteristic peaks at 1578 cm^{-1} and 1495 cm^{-1} can be ascribed to the C–C stretching deformation of quinoid and benzene rings, respectively [20]. Moreover, the bands in the 1200–1400 cm^{-1} correspond to the C–N stretching band of anaromatic amine and the N=Q=N stretching band at 1140 cm^{-1} is the characteristic band of polyaniline base. All these results reveal that polyaniline is formed in both composites.

XRD patterns of the pristine OBMC and the PANI/OBMC-60% and PANI/OUMC-60% composites are presented in Fig. 5. The OBMC yields three resolved diffraction peaks, indicating the well regular structure in the long-range. The intense diffraction peak and the other two weak peaks can be indexed as 100, 110, 200 reflections of a 2-D hexagonal symmetry with the space group of *p6m* [21], which is in accordance with the TEM results. Moreover, both composites exhibit similar patterns to the OBMC, except for a slight change in peak intensity. In general, the incorporation of guest species into the internal pores of mesoporous materials results in the decrease in the peak intensity [22]. Therefore, it can be concluded that the PANI polymer was introduced inside the primary mesopores. Furthermore, the shift of the diffraction peaks to lower angles for two composites can also be attributed to the introduction of the PANI.

N_2 adsorption/desorption isotherms and pore size distribution curves of OMC–SiO_2, OBMC, PANI/OBMC-60% and PANI/OUMC-60% were compared and shown in Fig. 6, and the corresponding pore characters are summarized in Table 1. All the samples exhibit type-IV curves with distinct capillary condensation steps, suggesting ordered mesoporous materials with narrow pore size distributions. A distinctly increased adsorption at relative pressure of 0.1–0.3 for OBMC (Fig. 6a) corresponds to smaller pores with a wide

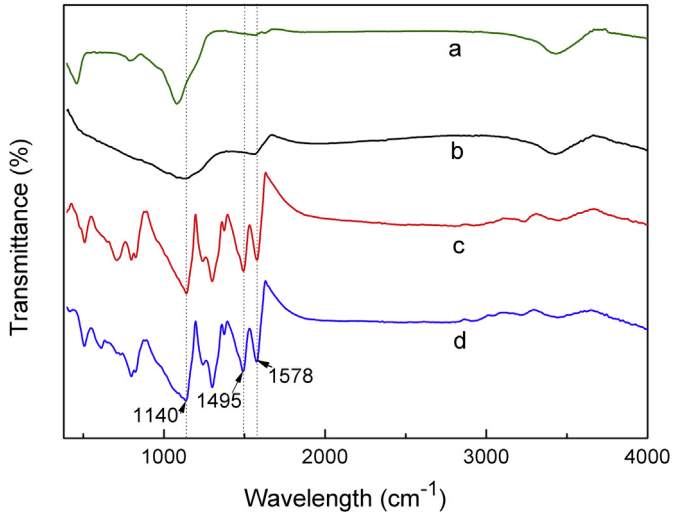

Fig. 4. FTIR spectra of (a) OMC–SiO_2, (b) OBMC, (c) PANI/OBMC-60% and (d) PANI/OUMC-60%.

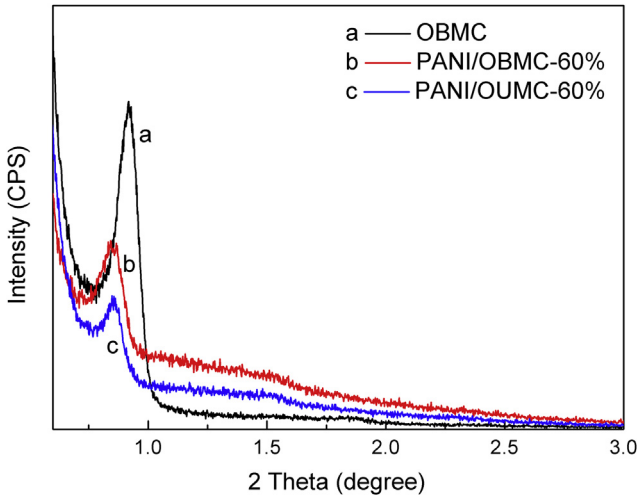

Fig. 5. XRD powder patterns of (a) OBMC, (b) PANI/OBMC-60% and (c) PANI/OUMC-60%.

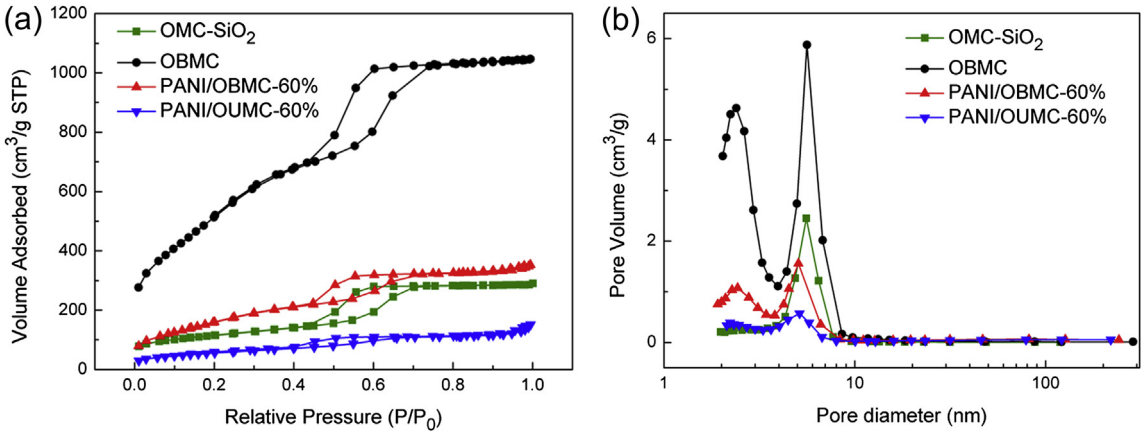

Fig. 6. (a) N_2 adsorption–desorption isotherms and (b) corresponding pore size distribution curves of OMC–SiO_2, OBMC, PANI/OBMC-60% and PANI/OUMC-60%.

distribution below 3.0 nm [16]. The bimodal pore structure of OBMC can be clearly found from Fig. 6b. The OBMC possesses the primary mesopore with a diameter at 5.6 nm and smaller mesopores centered at 2.4 nm. However, the OMC–SiO_2 only has 5.6 nm mesopores as a result of the degradation of the surfactants. Therefore, the smaller mesopores of 2.4 nm inside the carbon walls are caused by the removal of silica from the OMC–SiO_2 composites and endow the OBMC with high specific surface area of 1913 $m^2\ g^{-1}$ and large pore volume of 1.62 $cm^3\ g^{-1}$. After the incorporation of PANI into the OBMC, the surface area and pore size of PANI/OUMC-60% is decreased to 204 $m^2\ g^{-1}$ and 5.2 nm, respectively. The disappearance of pore distribution at 2.4 nm shows that the smaller mesopores were occupied with PANI. On the contrary, when OMC–SiO_2 as the host (synthetic route (a) in Fig. 1), the smaller mesopores of 2.4 nm were preserved after polymerization and the pore size of the primary mesopores of the carbon matrix in PANI/OBMC-60% decreased to 5.0 nm. Therefore, it can be concluded that a thin PANI layer of about 0.3 nm were coated on the inner surface of the primary mesopores [18] and the small mesopores on the carbon pore walls were effectively conserved in PANI/OBMC-60% composite.

3.2. Electrochemical properties

As with the well-aligned doping state of PANI nanowires and bimodal pore distribution, PANI/OBMC composites are expected to show excellent performance as supercapacitor electrode materials. In order to investigate the influence of PANI content on the capacitance performance, PANI/OBMC composites prepared in different aniline concentrations were measured by galvanostatic charge/discharge at 0.1 A g^{-1} (Fig. 7A). And the relationship between the specific capacitance (SC) of the PANI/OBMC nanocomposite and the weight percentage of PANI is plotted in Fig. 7B.

Table 1
Physicochemical properties of OMC–SiO_2, OBMC, PANI/OBMC-60% and PANI/OUMC-60%.

	S_{BET} ($m^2\ g^{-1}$)	S_m ($m^2\ g^{-1}$)	V_t ($cm^3\ g^{-1}$)	D_p (nm)	D_s (nm)
OMC–SiO_2	405	98	0.45	5.6	
OBMC	1913	457	1.62	5.6	2.4
PANI/OBMC-60%	599	148	0.55	5.0	2.4
PANI/OUMC-60%	204	15	0.23	5.2	

Notation: S_{BET}: total BET surface area; S_m: micropore surface area; V_t: total pore volume; D_p: primary mesopore diameter; D_s: small mesopore diameter.

The SC of electrode material is calculated according to the following equation:

$$C = \frac{2(I \times t)}{(m \times \Delta V)}$$

where C is specific capacitance (F g^{-1}), I is the charge–discharge current (A), t is the discharge time (s), m is the mass of active material within one electrode and the working voltage. The SC of the composite increases linearly with PANI content at low loading and reaches a maximum of 517 F g^{-1} at 60% PANI. As the loading of PANI further increases beyond 60%, the SC of the composite decreased dramatically. The decrease trend of SC with increasing PANI content can be explained that the primary mesopores occupied or blocked up by the excess PANI lead to a dramatic decline in the surface area, which can be confirmed by the physicochemical properties of the composites with high PANI content (Fig. S1 and Table S1 in Supplementary material).

The cyclic voltammogram (CV) curves of the OBMC, PANI/OBMC-60% and PANI/OUMC-60% were characterized at the scan rate of 10 mV s^{-1}. In Fig. 8a, the rectangle-shaped CV profile of OBMC shows a typical electric double layer capacitance (EDLC) while the two composites exhibit a couple of redox peak in their curves. Moreover, the PANI/OBMC-60% composite possesses a larger current density response compared to PANI/OUMC-60% electrodes at the same scan rate, indicating the largest specific capacitance of PANI/OBMC-60%. It can be concluded that the bimodal pore distribution of PANI/OBMC-60% with small mesopores in the carbon pore walls can effectively improve the capacitance of the electrode. Fig. 8b displays the CV curves of PANI/OBMC-60% composite measured at scan rates of 5, 10, 20 and 50 mV s^{-1}, respectively. It can be noted that all the CV profiles show similar shapes of anodic and cathodic peaks and the total peak current density increases with increasing the scan rate. This demonstrates a significant rate capability and excellent kinetic performance for the PANI/OBMC-60% nanocomposite.

To further confirm the merits of hierarchical composite as supercapacitor electrodes, the galvanostatic charge/discharge curves of OMC, OBMC, PANI/OBMC-60% and PANI/OUMC-60% were measured at a current density of 0.1 A g^{-1}. As can be seen from Fig. 8c, the OMC and OBMC electrode exhibit ideal double-layer capacitor behaviors from the typical triangular-shaped curve, while the charge/discharge curves of the PANI/OBMC-60% and PANI/OUMC-60% composites show two clear voltage stages: 0.45–0.8 V and 0.0–0.45 V, respectively. During the former, the relatively short charge–discharge duration is ascribed to pure EDLC; the

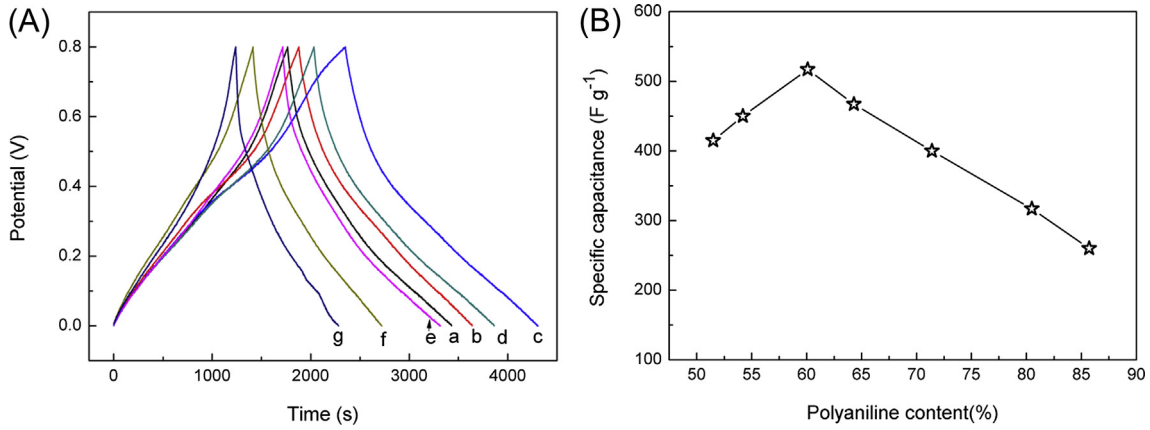

Fig. 7. (A) Galvanostatic charge–discharge curves of hierarchical composites with different PANI contents: (a) PANI/OBMC-51%, (b) PANI/OBMC-54%, (c) PANI/OBMC-60%, (d) PANI/OBMC-64%, (e) PANI/OBMC-71%, (f) PANI/OBMC-81% and (g) PANI/OBMC-86% at a current density of 0.1 A g^{-1}; (B) Influence of PANI content on the specific capacitance of PANI/OBMC composites.

longer charge–discharge duration in the latter is the combination of EDLC and faradaic capacitance. Due to its interconnected channels with improved ion diffusion, the SC of OBMC (195 F g^{-1}) with bimodal pore distribution is higher than that of OMC (148 F g^{-1}). Since the existence of PANI in composites, the gravimetric capacitance of PANI/OBMC-60% (517 F g^{-1}) and PANI/OUMC-60% (422 F g^{-1}) composites is superior to pure carbon material, which is in consistent with the result of CV tests.

Rate capability of two composites was investigated by charge–discharge measurements, shown in Fig. 8d. It is notable that the PANI/OBMC-60% electrode has higher capacity than PANI/OUMC-60% at various current densities. The capacitance retention of the PANI/OBMC-60% composite is 71.2% as current densities increase from 0.1 A g^{-1} to 5 A g^{-1}, whereas that of PANI/OUMC-60% is only 58% under similar condition, indicating the former composite electrode has better rate capability. The high specific capacitance

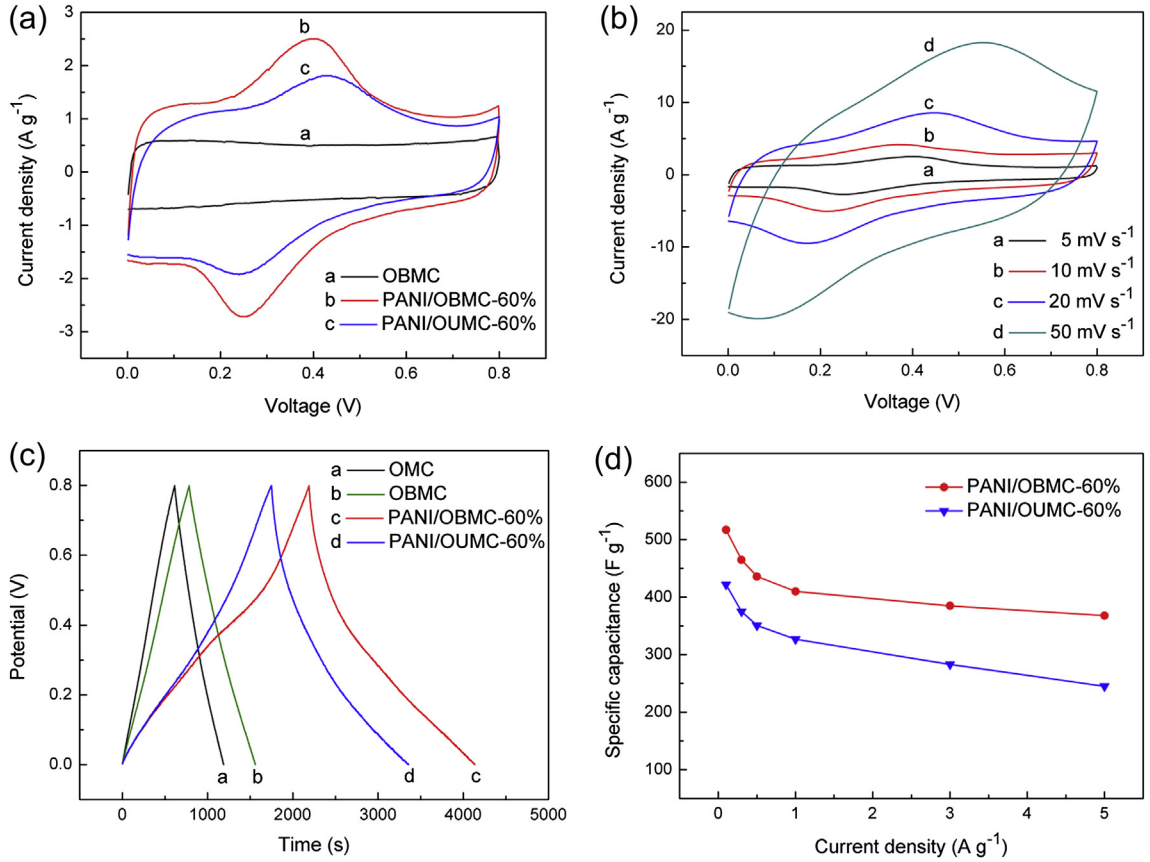

Fig. 8. (a) The cyclic voltammetry of OBMC, PANI/OBMC-60% and PANI/OUMC-60% at 10 mV s^{-1}; (b) CVs of PANI/OBMC-60% composite at different scan rates; (c) Galvanostatic charge–discharge curves of OMC, OBMC, PANI/OBMC-60% and PANI/OUMC-60% at a current density of 0.1 A g^{-1} and (d) specific capacitance of PANI/OBMC-60% and PANI/OUMC-60% at different current densities.

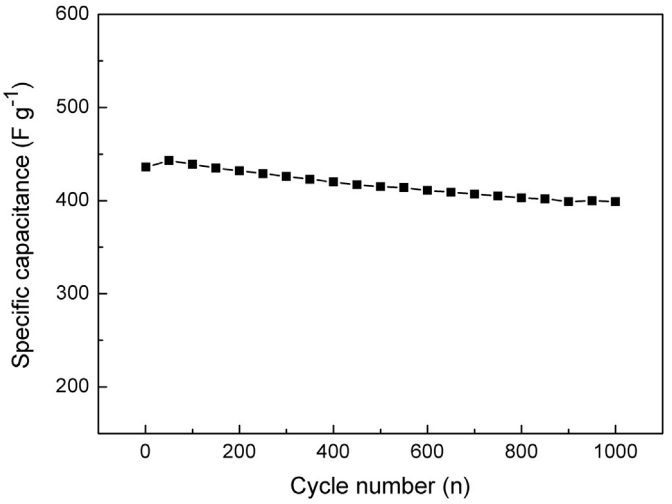

Fig. 9. Cycle performance of PANI/OBMC-60% under a current density of 0.5 A g^{-1}.

and good rate capability of PANI/OBMC-60% can be attributed to its unique structure. Firstly, the preserved small mesopores in the carbon walls endow the PANI/OBMC-60% with high surface area and large pore volume, resulting in an interpenetrating framework. Secondly, the inner surface of the mesochannels in PANI/OBMC-60% covered with hydrophilic PANI can be easily wetted by the aqueous electrolyte. And the thin layer of PANI on the inner surface can greatly shorten the diffusion and migration length of the electrolyte ions. Thirdly, when the portion of the incorporated PANI in composite is 60%, the primary mesopores reserved is large enough for the fast penetration of electrolyte. In addition, the unique hierarchical structure of the vertically aligned PANI nanowire arrays with OBMC can facilitate the ion diffusion from the electrolyte to the surface of the active materials in a short time. Meanwhile, the small diameter PANI nanowires can shorten the charge transfer distance, which ensure the high utilization of PANI.

The long-term cycle stability is also one of the most important factors influencing the electrochemical performance of electrode materials. In general, pure PANI often suffers from a limited long-term stability during cycling, which greatly restricts its commercial application. However, the composite combing PANI with OBMC is able to meliorate this shortcoming noticeably. The cycling stability of PANI/OBMC-60% composite electrode was examined by consecutive charge–discharge cycles at a current density of 0.5 A g^{-1} (Fig. 9). It can be observed that the specific capacitance of PANI/OBMC-60% composite first increases and then decreases slightly and still keeps 91.5% of its initial capacitance after 1000 cycles. The increased capacitance in the beginning can be interpreted as a result of the improvement of surface wetting between the electrode and the electrolyte during the cycling and the electroactivation process [23,24]. The good stability of PANI/OBMC-60% comes from the synergistic effect between PANI and OBMC. The OBMC substrate can prevent PANI from severely swelling and shrinking during the charge–discharge process. And facile strain relaxation in the vertical PANI nanowires effectively reduces the breaking of PANI chains during the doping/dedoping process of counterions [25,26]. Thus, the PANI/OBMC-60% nanocomposite with a good cycling stability can be a promising electrode material for supercapacitor applications.

4. Conclusions

PANI nanowire arrays were successfully incorporated into the OBMC on the premise of retaining the small mesopores on the pore walls and leaving the primary mesopores large enough. This novel hierarchical composite with bimodal pore distribution and hierarchical structure has a high surface area of 599 m^2 g^{-1}. Among the PANI/OBMC composites with PANI contents from 51% to 86%, the PANI/OBMC-60% has a maximum SC of 517 F g^{-1}, good rate capability and excellent cycle stability. The bimodal pore structure is in favor for the fast penetration of electrolyte and the unique hierarchical structure can facilitate the ion diffusion and shorten the charge transfer distance. Therefore, this novel hierarchical composite is a potential electrode material for energy storage.

Acknowledgments

This work was supported by the National Natural Science Foundation of China (20925621, 21236003, 21206043), the Shanghai Pujiang Program (12PJ1401900), the Fundamental Research Funds for the Central Universities and the Project sponsored by SRF for ROCS, SEM.

Appendix A. Supplementary data

Supplementary data related to this article can be found at http://dx.doi.org/10.1016/j.jpowsour.2013.03.190.

References

[1] B.E. Conway, Electrochemical Supercapacitors: Scientific Fundamentals and Technological Applications, Plenum, New York, 1999.
[2] M. Winter, R.J. Brodd, Chem. Rev. 104 (2004) 4245.
[3] V. Subramanian, H. Zhu, R. Vajtai, P.M. Ajayan, B. Wei, J. Phys. Chem. B 109 (2005) 20207.
[4] Y.G. Wang, Z.D. Wang, Y.Y. Xia, Electrochim. Acta 50 (2005) 5641.
[5] J.H. Park, J.M. Ko, O.O. Park, D.W. Kim, J. Power Sources 105 (2002) 20.
[6] K.R. Prasad, N. Munichand, J. Power Sources 112 (2002) 443.
[7] Y.K. Zhou, B.L. He, W.J. Zhou, J. Huang, X.H. Li, B. Wu, H.L. Li, Electrochim. Acta 49 (2004) 257.
[8] H. Zhang, G. Cao, W. Wang, K. Yuan, B. Xu, W. Zhang, J. Cheng, Y. Yang, Electrochim. Acta 54 (2009) 1153.
[9] B.K. Kuila, B. Nandan, M. Bohme, A. Janke, M. Stamm, Chem. Commun. (2009) 5749.
[10] H.S. Fan, H. Wang, N. Zhao, X.L. Zhang, J. Xu, J. Mater. Chem. 22 (2012) 2774.
[11] J.J. Xu, K. Wang, S.Z. Zu, B.H. Han, Z.X. Wei, ACS Nano 4 (2010) 5019.
[12] Y.G. Wang, H.Q. Li, Y.Y. Xia, Adv. Mater. 18 (2006) 2619.
[13] R. Ryoo, S.H. Joo, S. Jun, J. Phys. Chem. B 103 (1999) 7743.
[14] Y. Meng, D. Fu, F.Q. Zhang, Y.F. Shi, L. Cheng, D. Feng, Z.X. Wu, Z.X. Chen, Y. Wan, A. Stein, D.Y. Zhao, Chem. Mater. 18 (2006) 4447.
[15] R.L. Liu, Y.F. Shi, Y. Wan, Y. Meng, F.Q. Zhang, D. Gu, Z.X. Chen, B. Tu, D.Y. Zhao, J. Am. Chem. Soc. 128 (2006) 11652.
[16] H.Q. Li, R.L. Liu, D.Y. Zhao, Y.Y. Xia, Carbon 45 (2007) 2628.
[17] Y.R. Liang, D.C. Wu, R.W. Fu, Langmuir 25 (2009) 7783.
[18] Y.Q. Dou, Y.P. Zhai, H.J. Liu, Y.Y. Xia, B. Tu, D.Y. Zhao, X.X. Liu, J. Power Sources 196 (2011) 1608.
[19] Y. Meng, D. Gu, F.Q. Zhang, Y.F. Shi, H.F. Yang, Z. Li, C.Z. Yu, B. Tu, D.Y. Zhao, Angew. Chem. Int. Ed. 44 (2005) 7053.
[20] A.P. Monkman, P. Adams, Synth. Met. 40 (1991) 87.
[21] D.Y. Zhao, J.L. Feng, Q.S. Huo, N. Melosh, G.H. Fredrickson, B.F. Chmelka, G.D. Stucky, Science 279 (1998) 548.
[22] C.H. Kim, S.-S. Kim, F. Guo, T.P. Hogan, T.J. Pinnavaia, Adv. Mater. 16 (2004) 736.
[23] Q. Cheng, J. Tang, J. Ma, H. Zhang, N. Shinya, L.-C. Qin, Carbon 49 (2011) 2917.
[24] V. Ganesh, S. Pitchumani, V. Lakshminarayanan, J. Power Sources 158 (2006) 1523.
[25] Z.B. Lei, Z.W. Chen, X.S. Zhao, J. Phys. Chem. C 114 (2010) 19867.
[26] J.Y. Huang, K. Wang, Z.X. Wei, J. Mater. Chem. 20 (2010) 1117.